Bandgap Narrowing in Silicene Nanoribbons with Metal Edge Contacts

M. Poljak* and M. Matić
Computational Nanoelectronics Group
Micro and Nano Electronics Laboratory, Faculty of Electrical Engineering and Computing
University of Zagreb, HR-10000 Zagreb, Croatia
*E-mail: mirko.poljak@fer.hr

***Abstract*—By employing atomistic quantum transport simulations we investigate the impact of metal edge contacts on the transport gap (E_{TG}) of silicene nanoribbons (SiNR). Transmission and E_{TG} are investigated for sub-5 nm-wide and sub-15 nm-long SiNRs for various metal-device interaction strengths. We find that metallization occurs in certain cases, especially in wider and shorter devices, which sets fundamental limits to device scaling of potential SiNR-based field effect transistors (FET). The findings are elaborated through analytical and numerical examples by discussing transmission and eigenvalue evolution with increasing metal-device interaction.**

Keywords*—*silicene, nanoribbon, quasi-one-dimensional, bandgap, transport gap, bandgap narrowing, metallization, quantum transport, NEGF, wide-band limit, edge contact

I. Introduction

Silicene is a monolayer and monoelemental two-dimensional (2D) material similar to graphene with its Dirac linear dispersion in K points and zero bandgap, but with a somewhat buckled crystal lattice in contrast to the flat lattice of graphene [1]–[4]. Cutting silicene into nanoscale quasi-one-dimensional (1D) silicene nanoribbons (SiNRs) potentially allows denser device integration on chip and possibilities for adjusting material and device characteristics by quantum confinement [5], [6]. Material and device properties of SiNRs and SiNR field-effect transistors (FETs) have been investigated previously, although mainly for the case of ideal contacts [7]–[10]. Ideal contacts result in perfect step-like transmission characteristics because contact regions and the device are assumed to be made of identical materials, which turns off any scattering of electron waves at electrode-device interfaces [11]. Moreover, ideal contacts preserve the bandgap (E_G) while attaching realistic metal contacts changes the transmission function and induces a transport gap (E_{TG}) [12], [13]. Generally, $E_{TG} \neq E_G$ and it is crucial to study the effects of metal contacts on E_{TG} since the transport gap determines several fundamental figures-of-merit of FETs.

In this paper, we employ atomistic Hamiltonians coupled with the non-equilibrium Green's function (NEGF) formalism to study the electronic and transport properties, including E_{TG} behavior, of semiconducting SiNRs of various sizes. We investigate the impact of metal edge contacts since edge contacts are foreseen as a solution for better integration and lower contact resistance in ultra-scaled FETs based on 2D materials [14], [15]. An illustration of edge contacts for a SiNR FET is given in Fig. 1. Transmission and E_{TG} are analyzed for SiNR widths ranging from ~5 nm to ~0.5 nm, for nanoribbon lengths from ~15 nm to ~4.5 nm, and for different electrode metals modeled via a metal-device interaction strength parameter. We find that in certain cases SiNRs undergo metallization, i.e. transition from semiconductor to conductor, which limits the practical applicability of SiNRs of certain dimensions in extremely-scaled FETs.

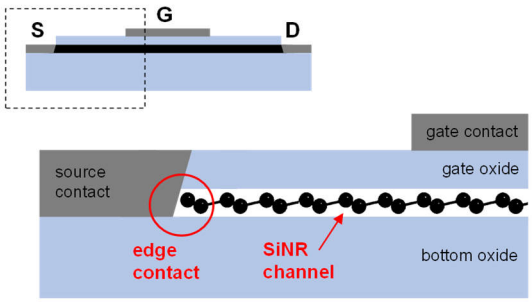

Fig. 1. Illustration of a SiNR FET (top) and a zoomed-in region on the source side showing a metal edge contact (bottom).

II. Methodology

In order to construct atomistic Hamiltonians for armchair-edge SiNRs we use the tight-binding (TB) model from the literature with nearest-neighbor interactions only where the Si-Si coupling or hopping parameter (t) for silicene is $t = 1.03$ eV [16]. Edge relaxation effect is accounted for by using a larger $t = 1.15$ eV for edge Si-Si bonds [7]. A 4-atom unit cell is constructed and repeated NW times along the nanoribbon width (W), which results in a column super-cell. This super-cell is then repeated NL times along the SiNR length (L), resulting in the total nanoribbon Hamiltonian matrix that contains $(4 \cdot NW \cdot NL)^2$ elements.

The focus of this study is on the bandgap, which can be extracted from the bandstructure, and more importantly on the transport gap, which is obtained from the energy-resolved quantum transmission function, $T(E)$, as the energy range where $T(E) < 0.001$. The E_{TG} is related to transport properties of a finite device and is therefore a more relevant figure-of-merit for potential device applications of ultra-scaled SiNRs. Transmission function of SiNRs is calculated within our existing NEGF code that deals with quasi-1D nanostructures such as nanoribbons of 2D materials [17]–[20]. The NEGF method starts by finding the retarded Green's function of the device, defined as

$$G^R(E) = \left[\left(E + i0^+\right) I - H - \Sigma_{C1}^R(E) - \Sigma_{C2}^R(E)\right]^{-1} \quad (1)$$

for a two-terminal nanodevice described by the TB Hamiltonian matrix H, while $\Sigma_C{}^R$ matrices are the retarded contact self-energies [21], [22]. The $\Sigma_C{}^R$ matrices account for open boundary conditions between the nanodevice, i.e. SiNR of a given size, and two electrodes. After calculating the retarded Green's function of the device, the transmission is found from

$$T(E) = Tr\left[\Gamma_{C1}(E)\, G^R(E)\, \Gamma_{C2}(E)\, G^A(E)\right] \quad (2)$$

where $G^A(E)$ is the advanced Green's function of the device, i.e. $G^A(E) = G^R(E)^\dagger$, and $\Gamma_C(E) = -2\,\mathrm{Im}\Sigma_C(E)$ is the contact-induced broadening for each electrode.

In the case of ideal contacts, the resulting transmission is a step-like curve, and $\Sigma_C{}^R$ matrices need to be calculated with an iterative algorithm, e.g. Sancho-Rubio method [22], [23]. On the other hand, in this work we are interested in how E_{TG} changes in SiNRs with metal edge contacts (MECs). The MECs are included by using the wide-band limit (WBL) approximation for reservoirs, which amounts to assuming metals with a constant density of states (DOS) and a constant metal-device coupling or hopping parameter (t_{MD}) [22]. The resulting $\Sigma_C{}^R$ matrices contain a single negative purely complex parameter (marked hereafter as $-\mathrm{Im}\Sigma_C{}^R$) since we neglect the real part and any energy shifts caused by attaching the metal electrodes. In order to assess a realistic magnitude of $-\mathrm{Im}\Sigma_C{}^R$ for an initial description of WBL contacts we use $\mathrm{DOS}(E = E_F) \sim 0.25\ \mathrm{eV}^{-1}$ similar to DOS of Au at Fermi level [24], and assume t_{MD} of 3 eV close to the coupling parameter for a graphene TB model. Hence, we obtain $-\mathrm{Im}\Sigma_C{}^R = t_{MD}{}^2 \cdot \mathrm{DOS}(E_F)/2 \approx 1.1$ eV and use $-\mathrm{Im}\Sigma_C{}^R = 1$ eV for initial simulations.

Later in the paper we examine the impact of reducing $-\mathrm{Im}\Sigma_C{}^R$ down to 0.1 eV, thus modeling a less interacting metal, and increasing $-\mathrm{Im}\Sigma_C{}^R$ up to 10 eV, which mimics metal electrodes with strong interaction towards the SiNR structure. The wide range of $-\mathrm{Im}\Sigma_C{}^R$ values that are explored comes from a study of graphene-metal and carbon nanotube-metal contacts that reported WBL interaction parameters ranging from ~0.01 eV for Pd electrodes to ~20 eV for Ni contacts [25], [26]. The wide range is a consequence of various DOS values at Fermi level in different metals, and of various coupling parameters between metals and graphene. In this work concerning SiNRs, the effects of attaching MECs with different interaction strengths $-\mathrm{Im}\Sigma_C{}^R$ are studied for various nanoribbon widths and lengths to assess the potential design space, i.e. allowed geometries of SiNRs in terms of the transport gap.

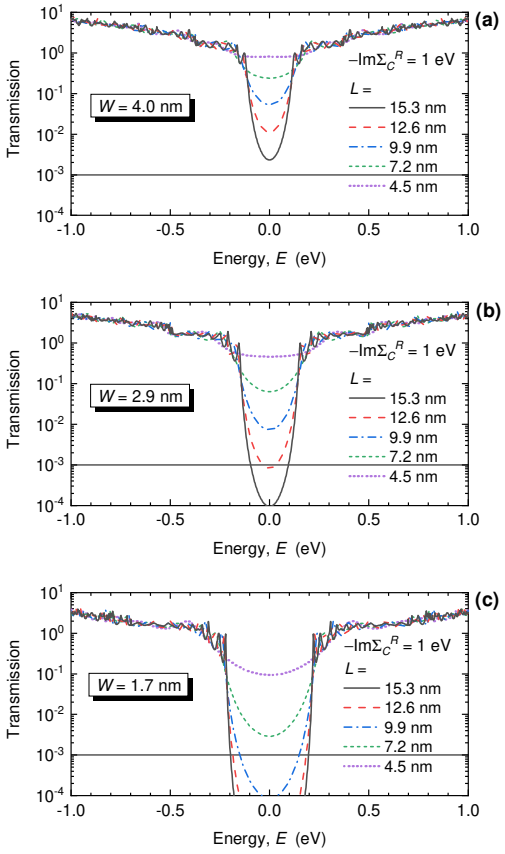

Fig. 2. Transmission vs. energy for (a) 4.0 nm-, (b) 2.9 nm-, and (c) 1.7 nm-wide SiNRs of different lengths with the metal-device interaction parameter of 1 eV.

III. Results and Discussion

First, we investigate the impact of attaching WBL metal edge contacts, with $-\mathrm{Im}\Sigma_C{}^R = 1$ eV as interaction parameter, on the transmission of 15.3 nm to 4.5 nm long SiNRs. Transmission characteristics for SiNR widths of 4.0 nm, 2.9 nm and 1.7 nm are plotted in Fig. 2a, b and c, respectively. Downscaling of SiNR width increases the bandgap and, consequently, the transport gap, which is easily visible for 15.3 nm-long structures in the central energy range where the transmission is suppressed considerably. However, the transmission does not cross the defined E_{TG} limit of $T(E) < 0.001$ in all cases. For $W = 1.7$ nm, E_{TG} exists for SiNRs that are at least 9.9 nm long. When L equals 4.5 nm and 7.2 nm the transmission is ~0.01 and ~0.1 at mid-gap, i.e. transport gap effectively closes and these 1.7 nm-wide SiNRs become metallized.

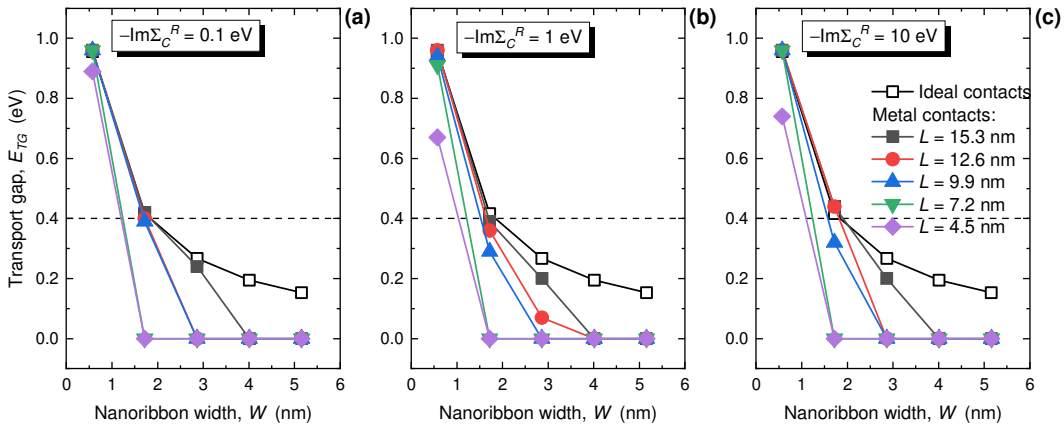

Fig. 3. Impact of SiNR width and length downscaling on the transport gap in SiNRs with metal edge contacts for various metal-device interaction strengths, i.e. with $-\mathrm{Im}\Sigma_C^R$ values of (a) 0.1 eV, (b) 1 eV, and (c) 10 eV. The characteristic of a SiNR with ideal contacts is inserted for comparison.

For $W = 2.9$ nm, metallization occurs even for longer nanoribbons so only for $L = 15.3$ nm and $L = 12.6$ nm a clear E_{TG} can be extracted. Strikingly, a clear transport gap completely disappears in the widest SiNR, with $W = 4.0$ nm shown in Fig. 2a, irrespective of the length. The widest structures with the smallest bandgap are, hence, more susceptible to metallization effects than the narrower ones, as reported previously for graphene and other 2D material nanoribbons [11], [13], [27]. In the shortest ($L = 4.5$ nm) 2.9 nm- and 4.0 nm-wide SiNRs the transmission at mid-gap is on the order of ~1, which indicates unacceptable tunneling and very poor switching between the ON and OFF states in SiNR FETs for logic applications. Therefore, attaching metal edge contacts with a realistic interaction parameter of $-\mathrm{Im}\Sigma_C^R = 1$ eV causes significant changes in the transmission, can close the transport gap, and sets limits to acceptable nanoribbon sizes for applications in nanodevices.

The extracted E_{TG} is reported in Fig. 3 for various SiNR widths and lengths, and for different metal-device interaction parameters to enable an easier comparison later in the text. The analyzed values of $-\mathrm{Im}\Sigma_C^R$ are 0.1, 1 and 10 eV and the corresponding results are presented in Fig. 3a, b and c, respectively. First, we focus on the initial value of the interaction parameter, i.e. $-\mathrm{Im}\Sigma_C^R = 1$ eV as shown in Fig. 3b. When SiNR width is scaled from 5.2 nm down to 0.6 nm, E_G increases from 0.15 eV to 0.96 eV in SiNRs with ideal contacts where $E_{TG} = E_G$. However, when MECs are attached, E_{TG} generally decreases with decreasing length, irrespective of the width. The 5.2 nm- and 4.0 nm-wide SiNRs with MECs are metallized regardless of the length. For $W = 2.9$ nm, the SiNR is semiconducting only for $L \geq 12.6$ nm, end even for these lengths the E_{TG} decreases from 0.27 eV (ideal contacts), over 0.2 eV ($L = 15.3$ nm), to 0.07 eV ($L = 12.6$ nm). The metallization effects become weaker for the two narrowest SiNRs with the widths of 1.7 nm and 0.6 nm. For $W = 1.7$ nm, only the shortest ($L = 4.5$ nm) nanoribbon has $E_{TG} = 0$ eV, whereas for $W = 0.6$ nm all SiNRs exhibit a transport gap irrespective of nanoribbon length. For the narrowest device the only significant effect of attaching MECs is E_{TG} decrease, or bandgap narrowing, from 0.96 eV to 0.67 eV when $L = 4.5$ nm (i.e. change of −30%). We can summarize the observed effects as metallization and bandgap narrowing being the strongest in wider and shorter nanodevices. The wide SiNRs have a small bandgap that is more susceptible to metallization-induced narrowing, whereas in short SiNRs metal electrodes are close and their interaction induces high local density of states and closes the gap [11]. The plot in Fig. 3 also contains a horizontal line showing $E_G = 0.4$ eV, which is the minimum acceptable bandgap for future extremely-scaled FETs [28]. Clearly, for technology nodes where channel lengths under ~10 nm are needed, only the narrowest ~0.6 nm-wide SiNR offers an appropriate bandgap. Although SiNRs have been experimentally reported [5], [29], [30], fabricating sub-1 nm-wide SiNRs on a wafer scale would present a serious challenge.

Next, different metals are studied and their impact on E_{TG} is shown in Fig. 3a for $-\mathrm{Im}\Sigma_C^R = 0.1$ eV, and in Fig. 3c for $-\mathrm{Im}\Sigma_C^R = 10$ eV. The former value describes a weakly-interacting metal or a moderately-interacting contacts with defects and other nonidealities on the metal-device interface that decrease the effective $-\mathrm{Im}\Sigma_C^R$. Surprisingly, Fig. 3a shows that an order of magnitude weaker interaction does not lead to significantly weaker metallization effects in comparison to Fig. 3b. In comparison to the case when $-\mathrm{Im}\Sigma_C^R = 1$ eV, for $-\mathrm{Im}\Sigma_C^R = 0.1$ eV the transport gap vanishes in one additional device, in the 2.9 nm-wide and 12.6 nm-long SiNR. For other devices with a preserved energy gap the impact of MECs is somewhat weaker for $-\mathrm{Im}\Sigma_C^R = 0.1$ eV than for the initial case, but E_{TG} is still lower than in ideal devices. Increasing the metal-device interaction parameter to 10 eV (Fig. 3c), which models a strongly-interacting metal, leads to similar effects as discussed previously. In comparison to the case of $-\mathrm{Im}\Sigma_C^R = 1$ eV, E_{TG} goes to zero for the SiNR with $W = 2.9$ nm and $L = 12.6$ nm. Other nanoribbons experience similar E_{TG} changes as in

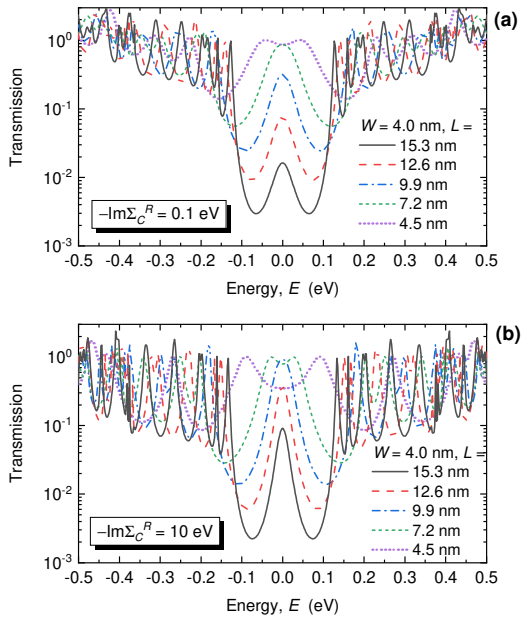

Fig. 4. Transmission of a 4.0 nm-wide SiNR of different lengths with the metal-device interaction parameter being (a) 0.1 eV, and (b) 10 eV.

the initial case of moderately-interacting metal electrodes defined by $-\mathrm{Im}\Sigma_C{}^R = 1$ eV.

The properties of E_{TG} in SiNR with weaker and stronger interactions are unexpected since one would expect a lesser E_{TG} change in Fig. 3a, and a larger impact of MECs in Fig. 3c, when compared to data presented in Fig. 3b for $-\mathrm{Im}\Sigma_C{}^R = 1$ eV. In order to clarify this issue, we plot the transmission for the 4.0 nm-wide SiNR with different lengths in the case of $-\mathrm{Im}\Sigma_C{}^R = 0.1$ eV in Fig. 4a and $-\mathrm{Im}\Sigma_C{}^R = 10$ eV in Fig. 4b. Both plots show that the transmission is greatly suppressed in the conduction and valence bands, with sharp transmission peaks occurring at specific energies. This result stands in stark contrast to step-like transmission characteristics of nanoribbons with ideal contacts, which is a signature of 1D and quasi-1D nanostructures [12], [26], [27]. In addition, the transmission increases inside the bandgap with decreasing nanoribbon length, in both cases. A similar effect was reported for graphene nanoribbons, with a pronounced peak at mid-gap that belongs to a strongly localized zero-energy state, i.e. metal-induced gap states (MIGS) are formed [12], [27]. This mid-gap increase due to MIGS is especially detrimental for SiNR FET operation as it would enhance direct tunneling through the channel and make the SiNR FET unable to turn off adequately.

As shown in supporting information of [13], assuming constant imaginary contact self-energies leads to Lorentzian-shaped transmission peaks at nanosystem eigenenergies. For example, the transmission of a simple one-level nanostructure equals

$$T(E) = \frac{1}{1+\left(E/\Gamma\right)^2} \qquad (3)$$

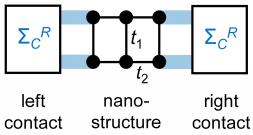

Fig. 5. Illustration of a quasi-1D nanostructure used for transmission analysis with respect to $-\mathrm{Im}\Sigma_C{}^R$. $t_1 = -3$ eV, $t_2 = -1$ eV.

for zero local energy, and with WBL contacts with $\Sigma_{C1} = \Sigma_{C2} = -\mathrm{i}\,\Gamma/2$. Hence, in realistic nanosystems with many eigenenergies, such as SiNRs, one can expect a transmission characteristic with a series of Lorentzians if WBL MECs are attached, which is exactly what is seen in Fig. 4. In devices such as SiNRs the individual Lorentzians are closely spaced due to a large number of states. Consequently, this crowding leads to overlaps and the local constructive interference causes transmission increase at certain energies.

Since SiNR is a relatively complicated system, it is easier to understand the evolution of transmission and E_{TG} with increasing $-\mathrm{Im}\Sigma_C{}^R$ using a 1D toy example. In the following analysis we assume a rectangular nanostructure that consists of two parallel 1D atomic chains, as illustrated in Fig. 5. The structure is a 2-by-3-atom nanoribbon with two WBL MECs that interact only with the two edge atoms on either side. For this system we increase the interaction parameter from 0.01 eV to 10 eV and plot the resulting transmissions in Fig. 6. For ideal contacts, the results assert that the nanostructure is a semiconductor with a 2 eV-wide bandgap and 4 eV-wide conduction and valence bands. However, with MECs the transmission changes significantly, with its shape evolving from delta-functions (Fig. 6a), over multiple Lorentzians in the bands (e.g. Fig. 6c), to a single Lorentzian in each band (e.g. Fig. 6h). The delta-functions, obtained for very weakly interacting MECs with $-\mathrm{Im}\Sigma_C{}^R = 0.01$ eV, indicate the localization or resonant regime with negligible transport probability, which means that the nanostructure is nearly isolated. Increasing $-\mathrm{Im}\Sigma_C{}^R$ to at least 0.1 eV increases the transmission to non-negligible levels. The six peaks that are visible in Fig. 6a-d are due to six states in the nanostructure. From Fig. 6e onwards, i.e. for $-\mathrm{Im}\Sigma_C{}^R$ equal to and higher than 1.3 eV, the separate peaks merge into one peak per band. This merging occurs because the contribution of contacts to system eigenvalues becomes dominant, which is seen in Fig. 7 that reports the real and imaginary parts of eigenvalues of the effective device Hamiltonian, $H_{eff} = H_0 + \Sigma$. The real part indicates where the transmission peaks occur, whereas the imaginary part defines the lifetime of a state via $\tau \sim \hbar / \mathrm{Im}(\varepsilon)$, where ε is a complex eigenvalue. The single peaks from Fig. 6e onwards become narrower as the interaction strength increases, in accordance with Eq. (3). For $-\mathrm{Im}\Sigma_C{}^R = 10$ eV (Fig. 6i) the Lorentzians are similar in shape to those obtained for $-\mathrm{Im}\Sigma_C{}^R = 0.1$ eV (Fig. 6b), but with a decreased number of peaks in the former case also comes an increased ETG of ~4 eV, in comparison to

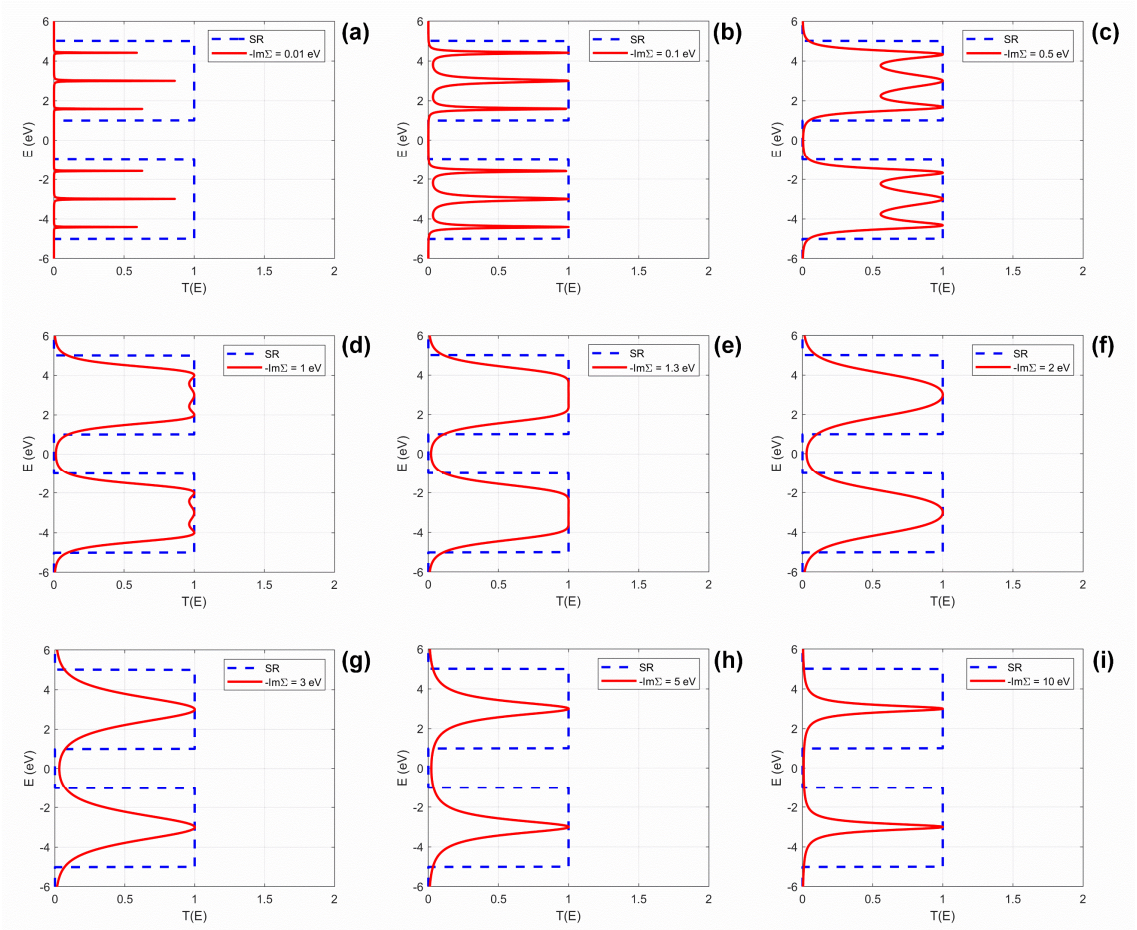

Fig. 6. Comparison of transmission functions of the device illustrated in Fig. 5 with ideal contacts (dashed line, obtained by the Sancho-Rubio (SR) method) and with metal edge contacts (full line). The nine plots show the impact of increasing $-\mathrm{Im}\Sigma_C^R$ from 0.01 eV to 10 eV.

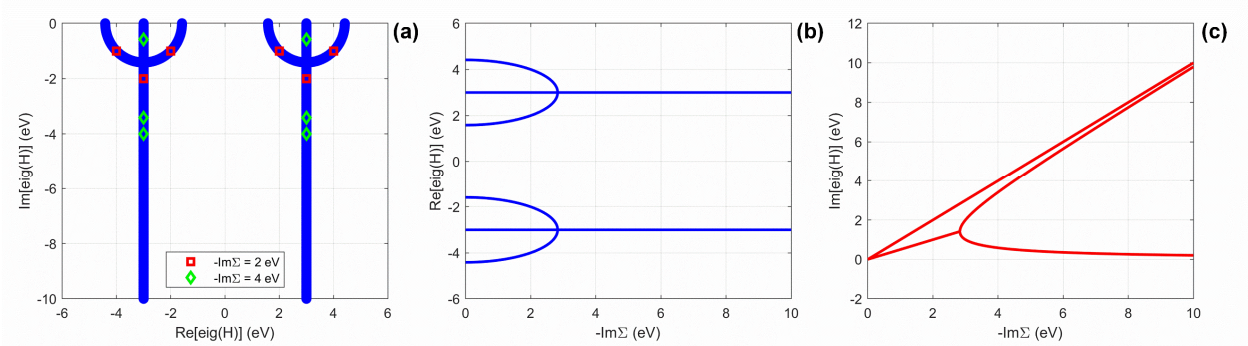

Fig. 7. (a) Eigenvalues in the complex plane for the effective Hamiltonian of the structure illustrated in Fig. 5 for various metal-device interaction strengths. Dependence of the (b) real and (c) imaginary part of the eigenvalues on $-\mathrm{Im}\Sigma_C^R$.

~3 eV when $-\mathrm{Im}\Sigma_C^R = 0.1$ eV, and 2 eV in SiNRs with ideal contacts. Therefore, this simplified analysis agrees with the findings on differences between Fig. 3a and c, i.e. stronger ETG narrowing is observed in the case of strongly-interacting metal edge contacts.

IV. Conlusions

Quantum transport simulations are employed to study metallization effects and bandgap narrowing in SiNRs with metal edge contacts. The analysis is done for various metal-device interaction strengths, and for technologically relevant SiNR dimensions, i.e. W under ~5 nm to reach relevant bandgap values, and L under ~15 nm for channels of future ultra-scaled FETs. We show that even moderately-interacting MECs ($-\mathrm{Im}\Sigma_C^R = 1$ eV) significantly suppress the transmission in the conduction and valence bands, increase the transmission inside the bandgap, cause considerable bandgap narrowing, and even metallization ($E_{TG} = 0$ eV). These MEC-induced effects set severe limits to scaling of SiNRs as channel material for FETs, e.g. SiNRs with $W > 3$ nm become metallized even when their length is ~15 nm. In addition, we demonstrate that weakly-interacting metals

($-\mathrm{Im}\Sigma_C^R << 1$ eV) could lead to localization regime with very poor transport properties and semiconductor-to-insulator transition. On the other hand, strongly-interacting metals ($-\mathrm{Im}\Sigma_C^R >> 1$ eV) can either decrease or further widen the transport gap, depending on the nanostructure and interaction strength. Overall, and specifically for SiNRs, only the sub-1 nm-wide devices are capable for length scaling down to ~5 nm due to the strong bandgap narrowing. These findings can be extended to other nanostructures with similar electronic properties and, therefore, could prove to be important for practical applications of 2D materials in nanoscale electron devices.

ACKNOWLEDGMENTS

This work was supported by the Croatian Science Foundation under the project CONAN2D (Grant No. UIP-2019-04-3493).

REFERENCES

[1] P. Vogt *et al.*, "Silicene: Compelling Experimental Evidence for Graphenelike Two-Dimensional Silicon," *Phys. Rev. Lett.*, vol. 108, no. 15, p. 155501, Apr. 2012, doi: 10.1103/PhysRevLett.108.155501.

[2] A. Kara *et al.*, "A review on silicene — New candidate for electronics," *Surface Science Reports*, vol. 67, no. 1, pp. 1–18, Jan. 2012, doi: 10.1016/j.surfrep.2011.10.001.

[3] K. S. Novoselov *et al.*, "Electric Field Effect in Atomically Thin Carbon Films," *Science*, vol. 306, no. 5696, pp. 666–669, Oct. 2004, doi: 10.1126/science.1102896.

[4] A. H. Castro Neto, F. Guinea, N. M. R. Peres, K. S. Novoselov, and A. K. Geim, "The electronic properties of graphene," *Rev. Mod. Phys.*, vol. 81, no. 1, pp. 109–162, Jan. 2009, doi: 10.1103/RevModPhys.81.109.

[5] P. De Padova *et al.*, "Evidence of graphene-like electronic signature in silicene nanoribbons," *Applied Physics Letters*, vol. 96, no. 26, pp. 261905-261905–3, Jun. 2010, doi: doi:10.1063/1.3459143.

[6] B. van den Broek, M. Houssa, A. Lu, G. Pourtois, V. Afanas'ev, and A. Stesmans, "Silicene nanoribbons on transition metal dichalcogenide substrates: Effects on electronic structure and ballistic transport," *Nano Res.*, vol. 9, no. 11, pp. 3394–3406, Nov. 2016, doi: 10.1007/s12274-016-1217-4.

[7] S. Kaneko, H. Tsuchiya, Y. Kamakura, N. Mori, and M. Ogawa, "Theoretical performance estimation of silicene, germanene, and graphene nanoribbon field-effect transistors under ballistic transport," *Appl. Phys. Express*, vol. 7, no. 3, p. 035102, Mar. 2014, doi: 10.7567/APEX.7.035102.

[8] M. A. Kharadi, G. F. A. Malik, K. A. Shah, and F. A. Khanday, "Sub-10-nm Silicene Nanoribbon Field Effect Transistor," *IEEE Transactions on Electron Devices*, vol. 66, no. 11, pp. 4976–4981, Nov. 2019, doi: 10.1109/TED.2019.2942396.

[9] M. Poljak, "Length-Dependent Electron Transport Properties of Defective Silicene Nanoribbons," *IEEE Transactions on Nanotechnology*, vol. 19, pp. 315–321, 2020, doi: 10.1109/TNANO.2020.2982071.

[10] M. Poljak, "Impact of Width Scaling and Parasitic Series Resistance on the Performance of Silicene Nanoribbon MOSFETs," *IEEE Trans. Electron Devices*, vol. 67, no. 11, pp. 4705–4708, Nov. 2020, doi: 10.1109/TED.2020.3017465.

[11] M. Poljak and M. Matić, "Metallization-Induced Quantum Limits of Contact Resistance in Graphene Nanoribbons with One-Dimensional Contacts," *Materials*, vol. 14, no. 13, p. 3670, Jan. 2021, doi: 10.3390/ma14133670.

[12] G. Liang, N. Neophytou, M. S. Lundstrom, and D. E. Nikonov, "Ballistic graphene nanoribbon metal-oxide-semiconductor field-effect transistors: A full real-space quantum transport simulation," *Journal of Applied Physics*, vol. 102, no. 5, p. 054307, Sep. 2007, doi: 10.1063/1.2775917.

[13] M. Poljak, M. Matić, T. Župančić, and A. Zeljko, "Lower Limits of Contact Resistance in Phosphorene Nanodevices with Edge Contacts," *Nanomaterials*, vol. 12, no. 4, Art. no. 4, Jan. 2022, doi: 10.3390/nano12040656.

[14] L. Wang *et al.*, "One-Dimensional Electrical Contact to a Two-Dimensional Material," *Science*, vol. 342, no. 6158, pp. 614–617, Nov. 2013, doi: 10.1126/science.1244358.

[15] A. Jain *et al.*, "One-Dimensional Edge Contacts to a Monolayer Semiconductor," *Nano Lett.*, vol. 19, no. 10, pp. 6914–6923, Oct. 2019, doi: 10.1021/acs.nanolett.9b02166.

[16] S. Cahangirov, M. Topsakal, and S. Ciraci, "Armchair nanoribbons of silicon and germanium honeycomb structures," *Phys. Rev. B*, vol. 81, no. 19, p. 195120, May 2010, doi: 10.1103/PhysRevB.81.195120.

[17] M. Poljak, E. B. Song, M. Wang, T. Suligoj, and K. L. Wang, "Influence of Edge Defects, Vacancies, and Potential Fluctuations on Transport Properties of Extremely Scaled Graphene Nanoribbons," *IEEE Trans. Electron Devices*, vol. 59, no. 12, pp. 3231–3238, Dec. 2012, doi: 10.1109/TED.2012.2217969.

[18] M. Poljak and T. Suligoj, "Immunity of electronic and transport properties of phosphorene nanoribbons to edge defects," *Nano Res.*, vol. 9, no. 6, pp. 1723–1734, Jun. 2016, doi: 10.1007/s12274-016-1066-1.

[19] M. Poljak, M. Glavan, and S. Kuzmić, "Accelerating simulation of nanodevices based on 2D materials by hybrid CPU-GPU parallel computing," in *2019 42nd International Convention on Information and Communication Technology, Electronics and Microelectronics (MIPRO)*, May 2019, pp. 47–52. doi: 10.23919/MIPRO.2019.8756964.

[20] M. Matić, T. Župančić, and M. Poljak, "Parallelized Ab Initio Quantum Transport Simulation of Nanoscale Bismuthene Devices," in *2022 45th Jubilee International Convention on Information, Communication and Electronic Technology (MIPRO)*, May 2022, pp. 118–123. doi: 10.23919/MIPRO55190.2022.9803335.

[21] S. Datta, *Electronic Transport in Mesoscopic Systems*. Cambridge University Press, 1997.

[22] M. Pourfath, *The Non-Equilibrium Green's Function Method for Nanoscale Device Simulation*. Wien: Springer-Verlag, 2014. doi: 10.1007/978-3-7091-1800-9.

[23] M. P. L. Sancho, J. M. L. Sancho, J. M. L. Sancho, and J. Rubio, "Highly convergent schemes for the calculation of bulk and surface Green functions," *J. Phys. F: Met. Phys.*, vol. 15, no. 4, p. 851, 1985, doi: 10.1088/0305-4608/15/4/009.

[24] K. Schwarz and P. Blaha, "DFT calculations of solids in the ground state," in *DFT calculations of solids in the ground state*, De Gruyter, 2018, pp. 67–100. doi: 10.1515/9783110433920-003.

[25] A. Fediai, D. A. Ryndyk, and G. Cuniberti, "The modular approach enables a fully ab initio simulation of the contacts between 3D and 2D materials," *J. Phys. Condens. Matter*, vol. 28, no. 39, p. 395303, 05 2016, doi: 10.1088/0953-8984/28/39/395303.

[26] A. Fediai *et al.*, "Towards an optimal contact metal for CNTFETs," *Nanoscale*, vol. 8, no. 19, pp. 10240–10251, May 2016, doi: 10.1039/C6NR01012A.

[27] G. Liang, N. Neophytou, M. S. Lundstrom, and D. E. Nikonov, "Contact Effects in Graphene Nanoribbon Transistors," *Nano Lett.*, vol. 8, no. 7, pp. 1819–1824, Jul. 2008, doi: 10.1021/nl080255r.

[28] F. Schwierz, J. Pezoldt, and R. Granzner, "Two-dimensional materials and their prospects in transistor electronics," *Nanoscale*, vol. 7, no. 18, pp. 8261–8283, Apr. 2015, doi: 10.1039/C5NR01052G.

[29] N. F. Kleimeier *et al.*, "Unoccupied electronic band structure of pentagonal Si nanoribbons on Ag(110)," *Phys. Chem. Chem. Phys.*, vol. 21, no. 32, pp. 17811–17820, Aug. 2019, doi: 10.1039/C9CP02239B.

[30] S. Yue *et al.*, "Observation of One-Dimensional Dirac Fermions in Silicon Nanoribbons," *Nano Lett.*, vol. 22, no. 2, pp. 695–701, Jan. 2022, doi: 10.1021/acs.nanolett.1c03862.